Stockholm University

Bachelor Thesis

Degree Project in Geology 15 hp

Analysis and identification of the formation and geological setting of rock samples from the DeLong Islands

Jacob Brotherton

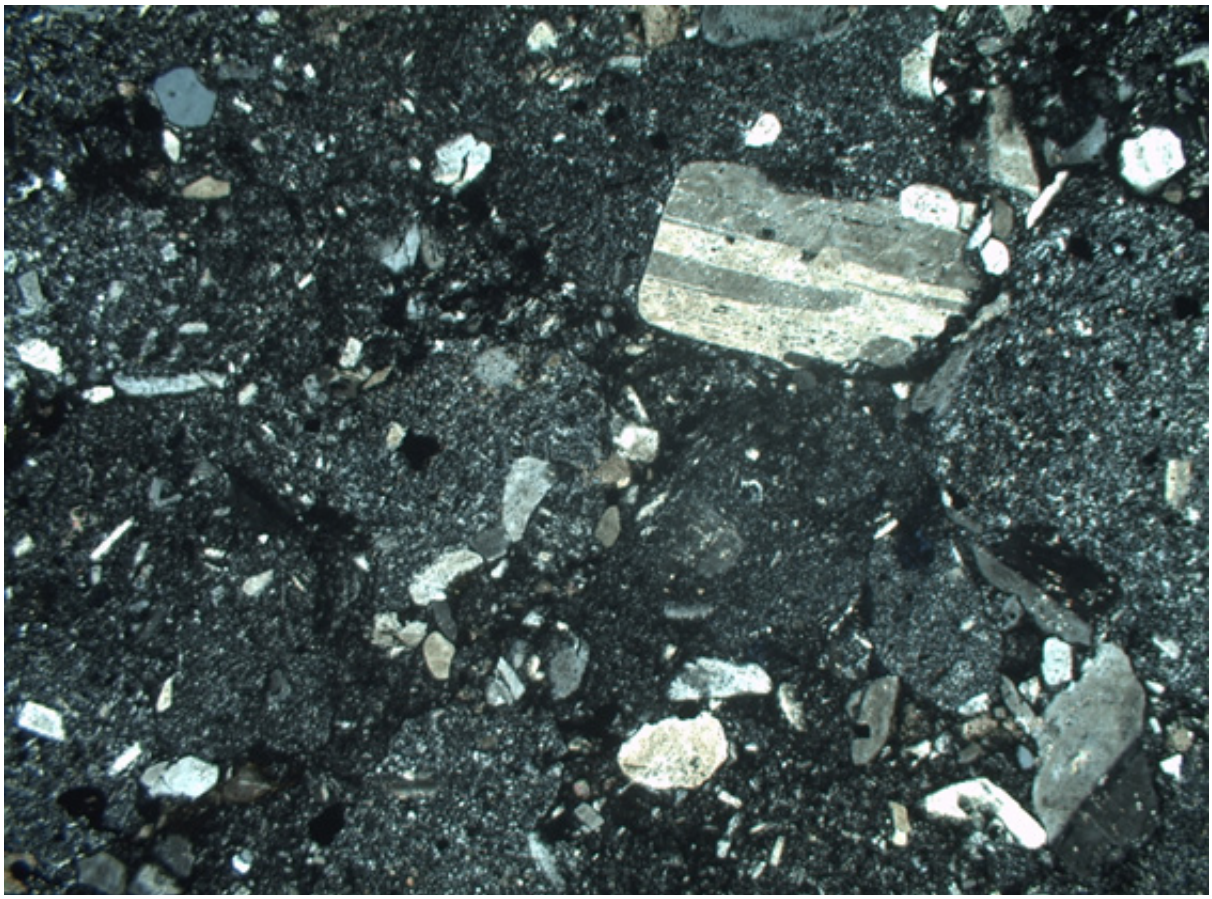

Stockholm 2014

Department of Geological Sciences
Stockholm University
SE-106 91 Stockholm

Abstract

The De Long Islands are a separate archipelago accommodated as part of the larger group of New Siberian Islands situated between the Laptev Sea in the West and the East Siberian Sea to the East. The De Longs form the North East section of the New Siberian Islands, as seen in figure 1. Henrietta Island, from which the samples studied in this thesis were collected from, is the northernmost Island in the archipelago. Geochemical and thin section analysis was conducted on the samples, to confirm whether previous assumptions that the rocks on Henrietta were derived from an oceanic arc complex were correct and to find out more detail about them. Henrietta island was confirmed to be the location of ocean arc derived igneous rocks as samples display typical arc signatures in multi element plots. The samples collected showed evidence of being derived from a depleted mantle source as confirmed by trace element analysis and multi element plots. The samples were formed in relatively close proximity to the subduction zone of this island arc, these samples were produced over a time span during which the arc continued to mature from initially being relatively immature. Fluids derived from the subducting oceanic crust were also instrumental in the formation of these rocks.

Table of Contents

Introduction

1.1 Aim of Study

The principle aim of this study is to expand our knowledge on the various igneous and volcanoclastic rocks of the De Long Islands through a variety of methods. The De Long Islands themselves are included as a part of the New Siberian Islands; a collection of islands situated off the North East coast of Siberia, Russia. Due to the extremely isolated setting of these islands and the difficulty in accessing them, only limited geological information is available; both in terms of the type of rocks seen and the geological setting they formed in. The samples analysed in this study are from Henrietta Island. Therefore this study is intended to confirm and expand upon field observations taken whilst on Henrietta and previous studies.

This is to be done by a combination of geochemical analysis, both XRF and ICP-MS conducted at Stockholm University, and complimented by the study of thin sections of the samples collected from Henrietta Island. The samples collected contained examples of purely igneous rocks along with examples of volcanogenic sediments. These sediments contained such a high igneous content they could be treated as igneous rocks when it came to geochemical analysis. Previous study has indicated that the igneous rocks and associated volcanoclastic units on Henrietta Islands are associated with the formation of an oceanic island arc complex (KOS'KO M. , 2009) and this paper will endeavour to ratify these assumptions. Furthermore, in addition to confirming that these igneous rocks are the products of oceanic subduction related volcanics, the genesis of these rocks will be studied. The processes that were involved in forming these rocks will be studied, with a focus on the source.

The total number of samples collected for analysis that were deemed suitable to be used is only seven. This is a very small number in terms of performing statistical analysis and confirming the results with any certainty however it is enough to diagnose the geological setting to some accuracy.

1. *Geological Background*

The De Long Islands are a separate archipelago accommodated as part of the larger group of New Siberian Islands situated between the Laptev Sea in the West and the East Siberian Sea to the East.

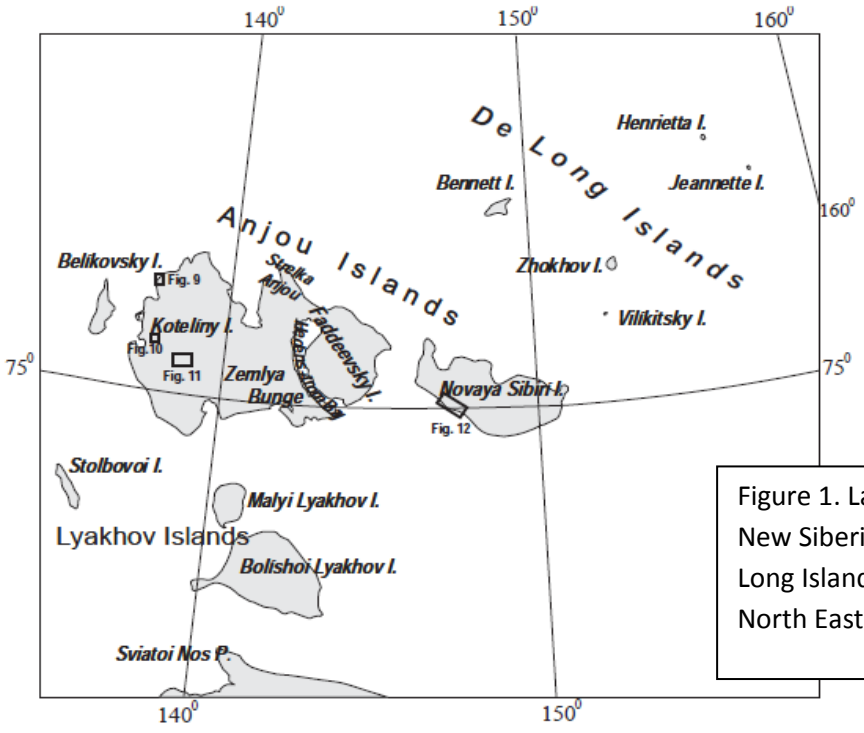

Figure 1. Large scale map of the New Siberian Islands, with the De Long Islands situated towards the North East. (KOS'KO M. , 2009)

The De Longs form the North East section of the New Siberian Islands, as seen in figure 1. Henrietta Island, from which the samples studied in this thesis were collected from, is the northernmost Island in the archipelago (KOS'KO M. , 2009).

There are four distinct geological units on Henrietta Island: the first being quartz sandstone, followed by two distinct tuffaceous layers: the first one is defined by rhythmic tuff-argillite with sandstones and the second is a tuffaceous gritstone-sandstone interbedded with siltstones. The final unit is igneous containing; tuff and lava, and basalt. The latter unit is in tectonic contact with the other units due to its intrusive nature in some places. Beds are folded into small asymmetrical folds around 1.5m in size which are broken into individual boudins, are over- turned, and are steeply dipping. 'Microline granite, gneiss, and micropegmatite clasts were reported from the upper half of the tuffaceous gritstone-sandstone unit. The whole section displays numerous sheets, sills and dykes of andesite-basalt, basalt, dolerite and dolerite-porphyrite' (KOS'KO, LOPATIN, & GANELIN, 1990). The folding and deformation has been associated with both local sediment deformation during lithification and larger scale deformation as part of the hypothesised Arctic Phanerozoic fold belt (KOS'KO M. , 2009) or later cretaceous rifting in the arctic (KUZMICHEV & PEASE, 2007).

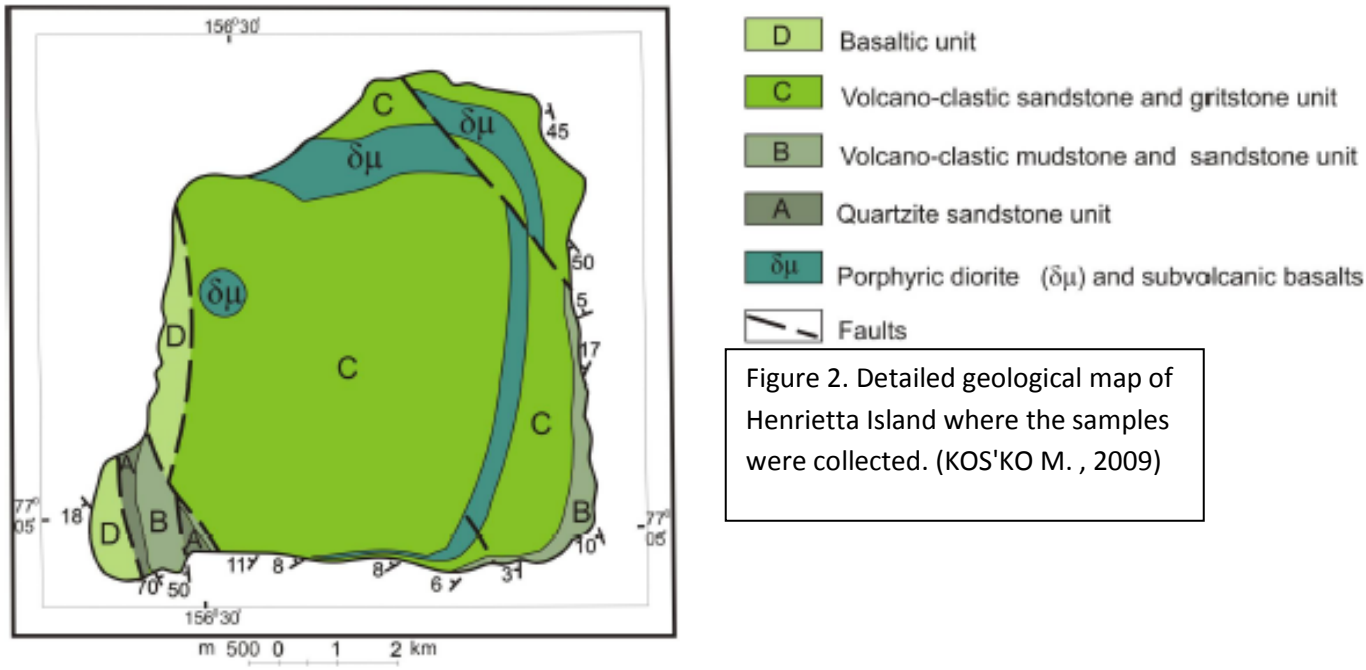

Figure 2. Detailed geological map of Henrietta Island where the samples were collected. (KOS'KO M. , 2009)

Dating of these rocks has shown some discrepancies across different papers but is regarded to be of Cambrian age, which was correlated by zircon dating of some samples also taken from Henrietta Island on the same expedition at 570-590 Ma (Pease, 2014).

2. Thin Section Summary

These petrological descriptions cover a selection of the samples from the igneous unit and both of the tuffaceous units. The slides selected aim to show a representation of the most interesting and diagnostic features seen across the samples.

DL13-09

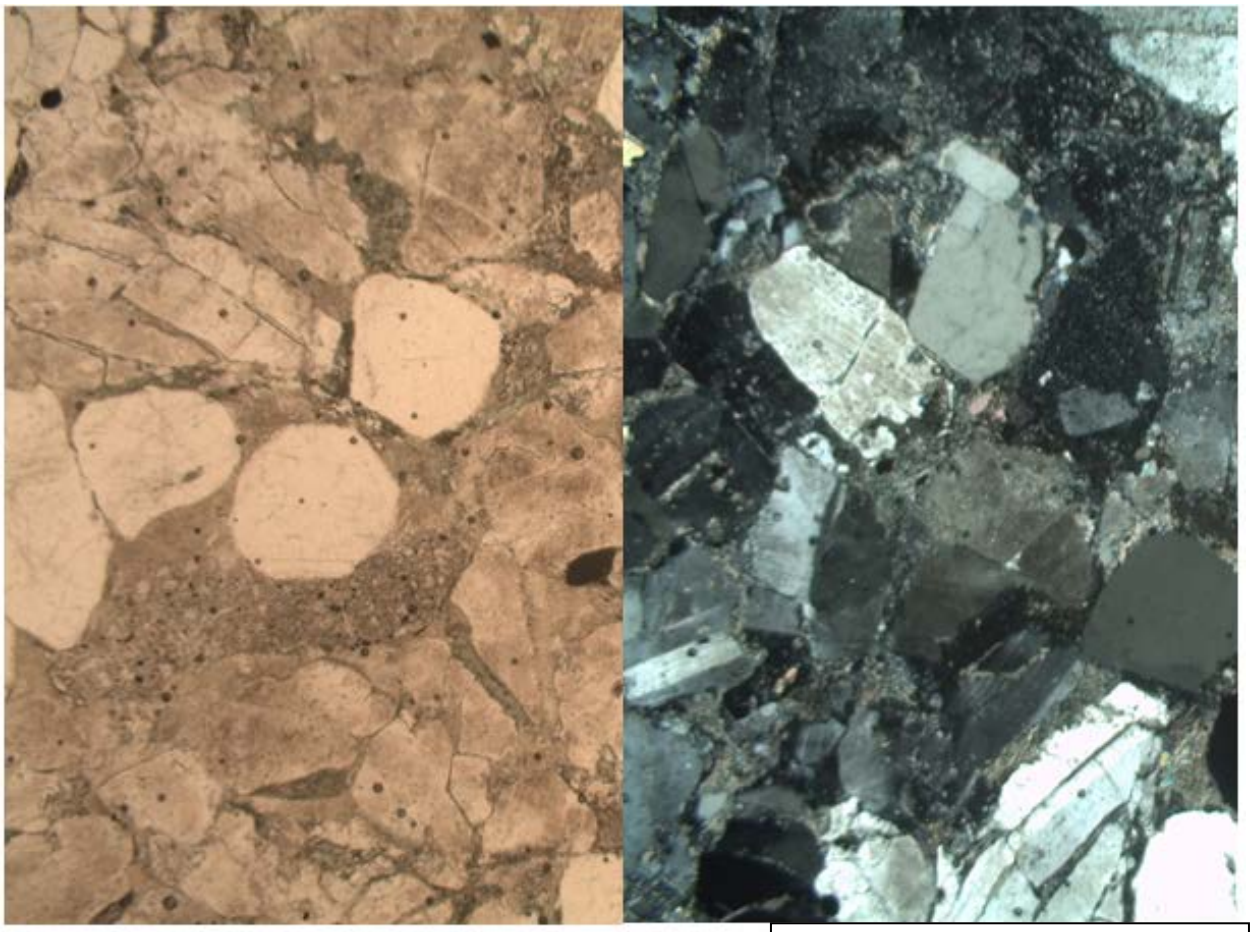

Figure 3. Magnified view (x4) of thin section of sample DL13-09. PPL (Plane Polars) on the left and XPL (Cross Polars) on the right.

Volcano Clastic Sandstone

The primary minerals in this sample are in order of abundance; plagioclase feldspar and quartz with minor amounts of clinopyroxene. The plagioclase crystals are mostly angular with few examples of perfect tabular form. The size of the crystals is up to 1.5mm in size in this thin section; relatively large compared to the majority of other samples.

The quartz crystals are generally rounded suggesting transport before deposition and lithification. This quartz content of this rock is quite high, which is not compliant with the majority of rocks associated with ocean island arc magma suites.

In addition to the primary minerals scattered throughout the slide are numerous lithic fragments. These lithic fragments are generally of basaltic composition with well-formed plagioclase laths. This further reinforces the evidence of transportation before deposition.

There is extensive secondary alteration of this rock, with chlorite, epidote and calcite seen throughout the section. Many larger plagioclase crystals have undergone sassuritisation; with the ferromagnesian components of the plagioclase crystals responsible for the formation of chlorite and epidote.

DL13-11

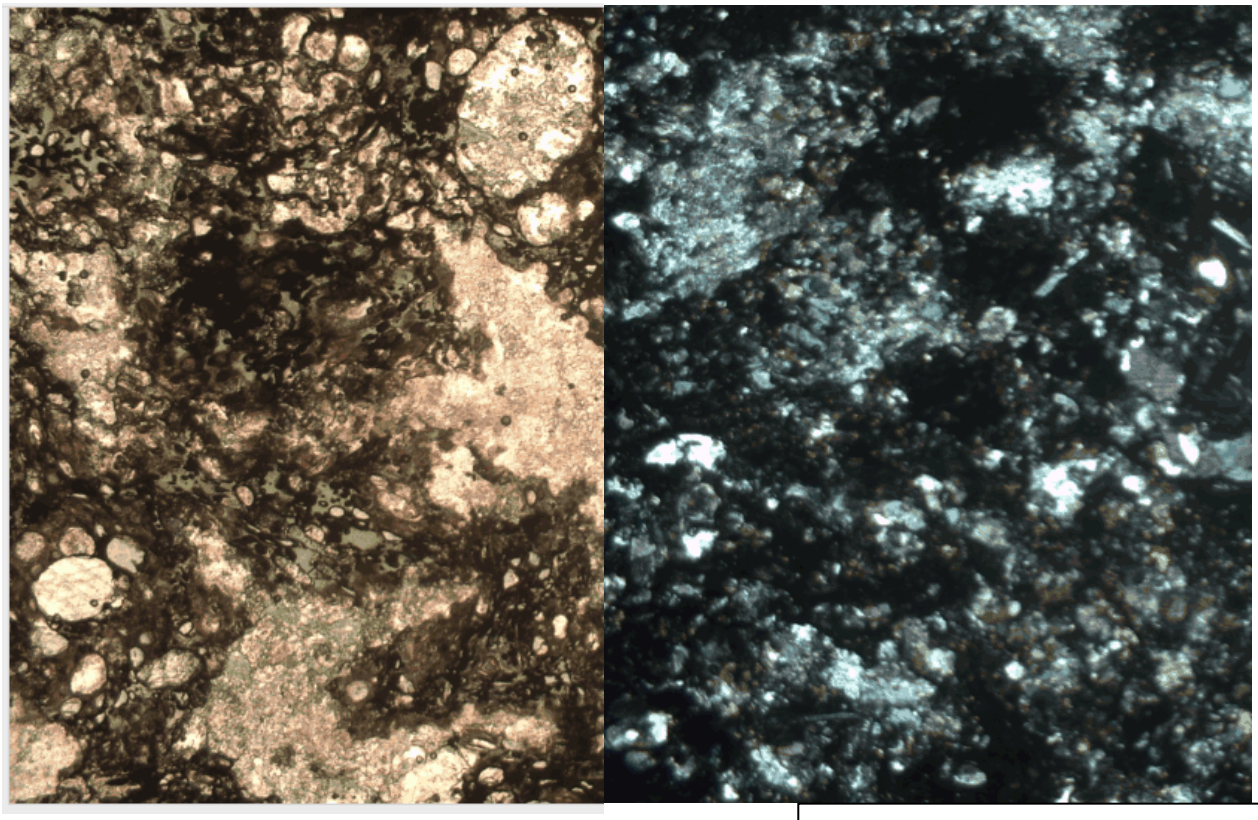

Figure 4. Magnified view (x4) of thin section of sample DL13-11. PPL on the left and XPL on the right.

Relic Tuff

This sample is an example of relic tuff that has undergone alteration. There are glass shards throughout this sample, in some places devitrification of the glass shards can be seen. Foliation is not pervasive across the sample but in isolated fragments.

There is extensive sericitisation across the sample, with many patches of clay minerals which could be an indicator of relic plagioclase crystals. However there are some plagioclase crystals that remain relatively unaltered and in good condition. Numerous different lithic fragments are visible throughout, including some of basaltic composition and some with higher quartz content. Along with numerous vesicles, some infilled with calcite and other secondary minerals associated with low grade metamorphism.

DL13-13XX

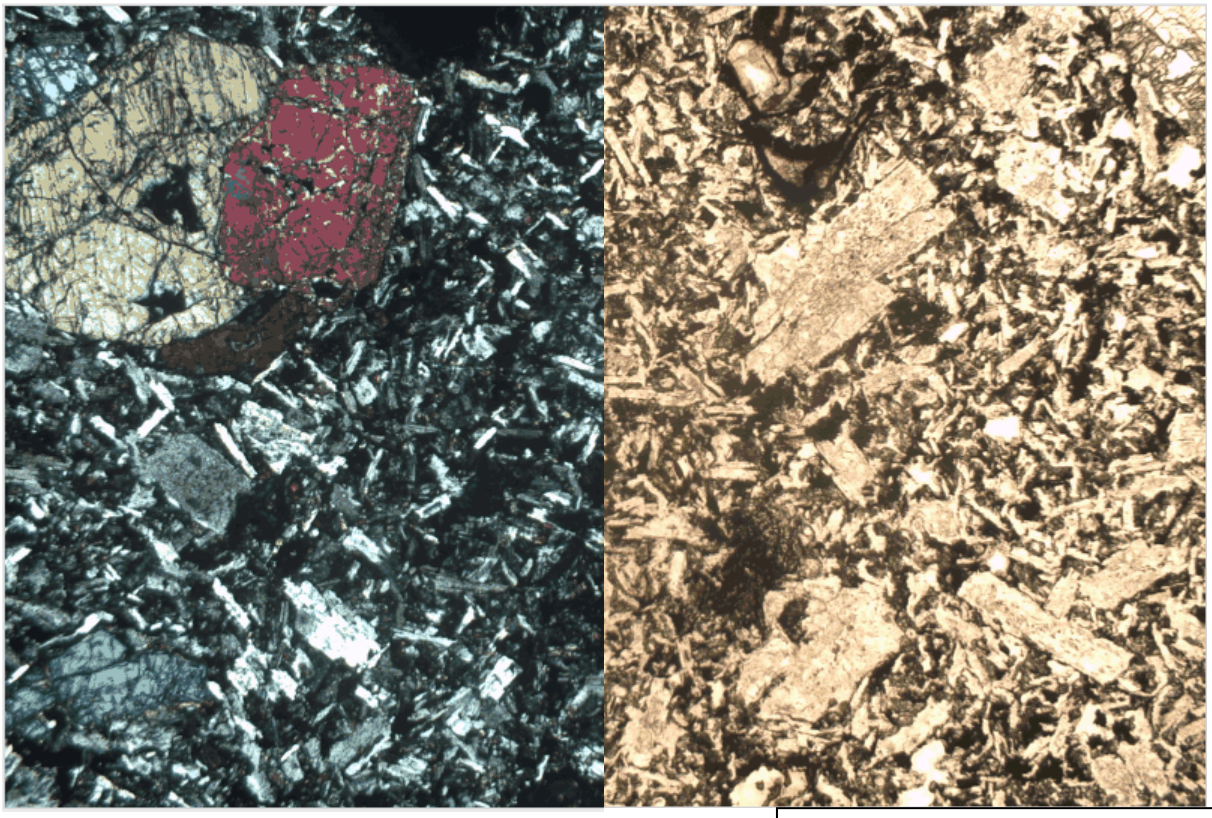

Figure 5. Magnified view (x4) of thin section of sample DL13-13XX. XPL on the left and PPL on the right.

Basalt

This basalt has a plagioclase feldspar groundmass with small crystal laths showing clear twinning. Plagioclase is the main component of this sample, however it is not just the constituent of the groundmass; there are also much larger plagioclase phenocrysts throughout the sample.

The other conspicuous phenocrysts in this thin section are the large clumps of pyroxenes, with crystals up to 3mm. These clumps of pyroxene phenocrystals are pervasive throughout the slide, with the main pyroxene being clinopyroxene yet there are still large examples of orthopyroxene as seen in figure 5. In some of these phenocrysts growths rims can be seen, combined with their large size could be indicative of a long time spent in a magma chamber or slow cooling rates.

There are also a number of opaque minerals in this section which could likely be various iron oxide minerals. Few examples of highly fractured olivine are also seen in the section.

This sample is also one of the least altered, with only small amounts of secondary minerals and few phenocrysts showing breakdown textures.

Method

There was considerable preparation involved in processing the collected samples, which took place at both Stockholm University and Stockholm's Natural History Museum. The samples were first split and crushed into gravel. Throughout these steps rock fragments showing high alteration, such as weathered surfaces and secondary veins were discarded so as to keep the whole rock powder as representative of the original igneous component as accurate as possible. After a whole rock powder had been generated from the samples it was taken to Stockholm University for geochemical analysis of major and trace elements using XRF and LA-ICPMS respectively. The analysis was only carried out after the samples were treated for 24 hours in a kiln at 1000°C to remove structurally bound water and other volatiles. From the difference in weight the LOI (Loss on ignition) was calculated and can be seen in figure 6.

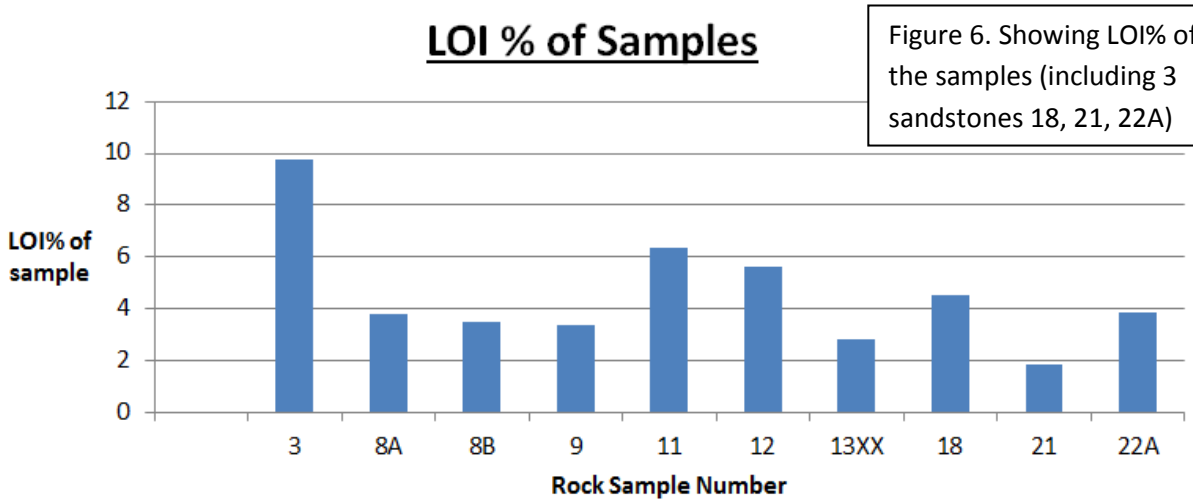

Figure 6. Showing LOI% of all the samples (including 3 sandstones 18, 21, 22A)

The values obtained for LOI's indicate a very high degree of hydrous minerals (H_2O that is bound within the crystal structure). With values over 8% for mafic rocks and over 4% for felsic and intermediate rocks considered anomalously high (Harris, Wilkinsona, & Grunsky, 2000) putting a number of the samples in the anomalous zone. This has an effect on the analysis of the results of these rocks, where it must be taken into consideration the mobility of the elements used to diagnose the rock. High LOI counts indicate alteration, alteration can mobilise mobile elements and change the sample's chemistry. Therefore when dealing with these rocks, as a number of them are altered, immobile elements will be used for analysis whenever possible. Also included in figure 6 are three sandstone samples (18,21,22A) showing alteration is not limited to the igneous samples.

Accuracy and precision of ICP-MS between 3-7% is considered to be good (Jenner, Longerich, Jackson, & Fryer, 1990) the relative standard deviation is advised to be kept below 6.5% (Wang, Yin, Zeng, Yang, & Chen, 2014). The majority of readings provided satisfactory results, with most relative standard deviations being under 10% and a great number of them being under 5% however there were a number of unconformable results such as the RSD of Cu being over 10% for most samples tested which indicates care must be taken when using these results. All readings were repeated three times for improved accuracy.

Results

$Na_2O + K_2O$ vs SiO_2 (wt%)

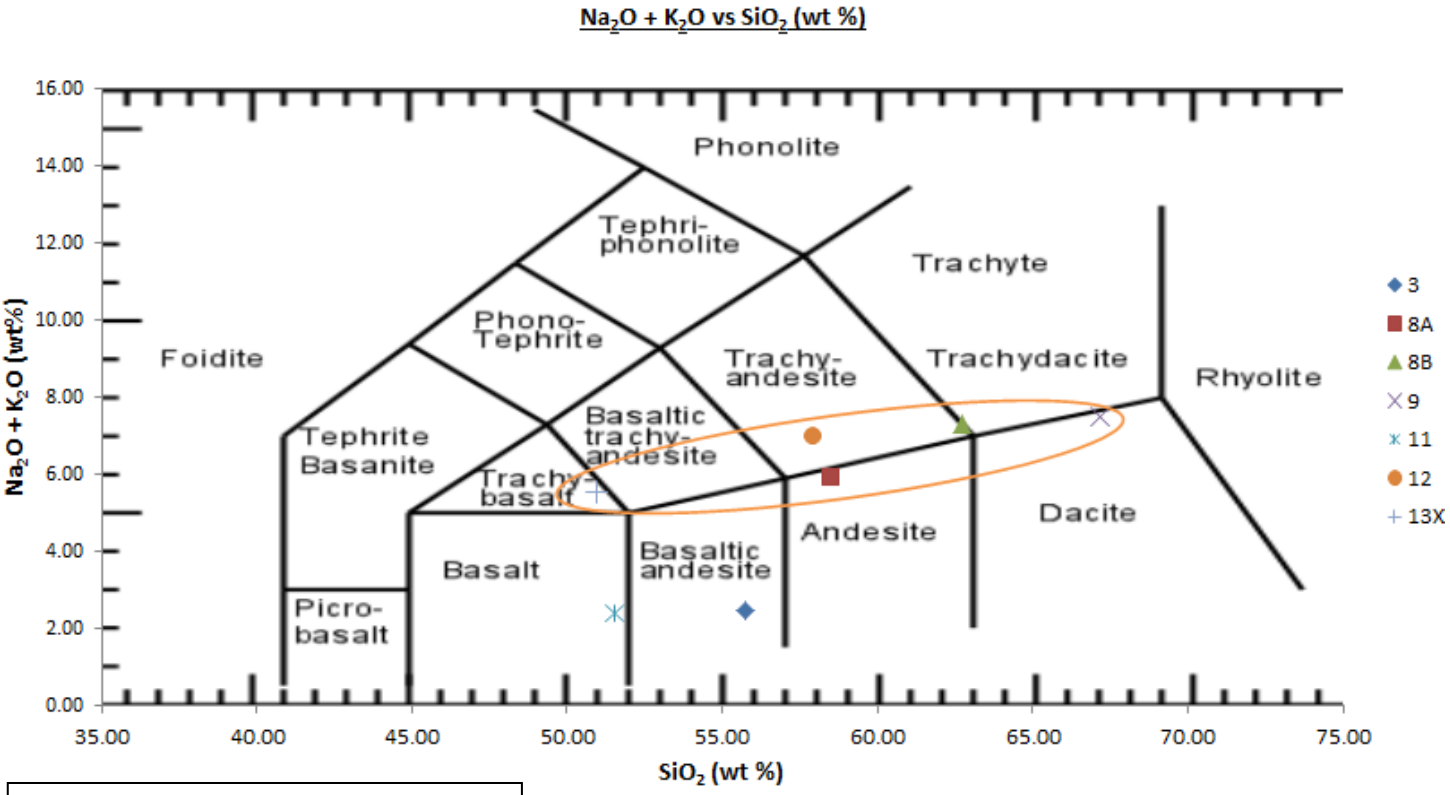

Figure 7. Alkali wt % versus Silica wt %

This plot shows Silica weight percent against a combination of Sodium and Potassium, allowing us to name our rock samples. Both samples 11 and 3 show a low alkali count, along with relatively low silica content. The other five samples have been highlighted in this figure as they seem to form a relatively clear trend. With the majority of these five having a high enough alkali content to be just situated in the trachyitic field. There is a wide spread of silica content throughout the whole samples.

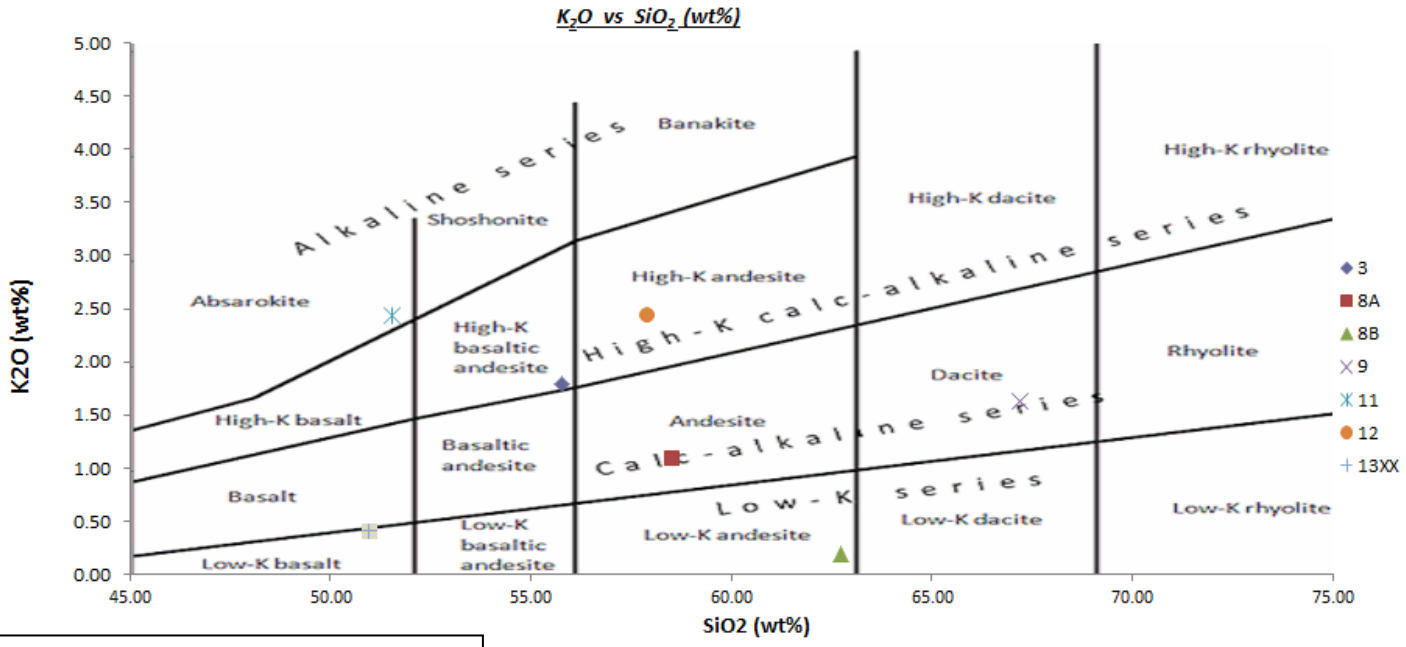

Figure 8. Potassium against silica wt %

This graph is intended to show which K series the rocks belong to, however due to the alteration of the rocks post lithification and K being a mobile element, the results are scattered and show no clear trend. With two samples in each of the Low-K, Calc-alkaline and High-K series and one sample plotting in the Alkaline series, this is where the low sample number proves problematic; there are not enough samples to say with any confidence these are separate trends or have been affected by varying degrees of alteration.

Alkali Lime Index

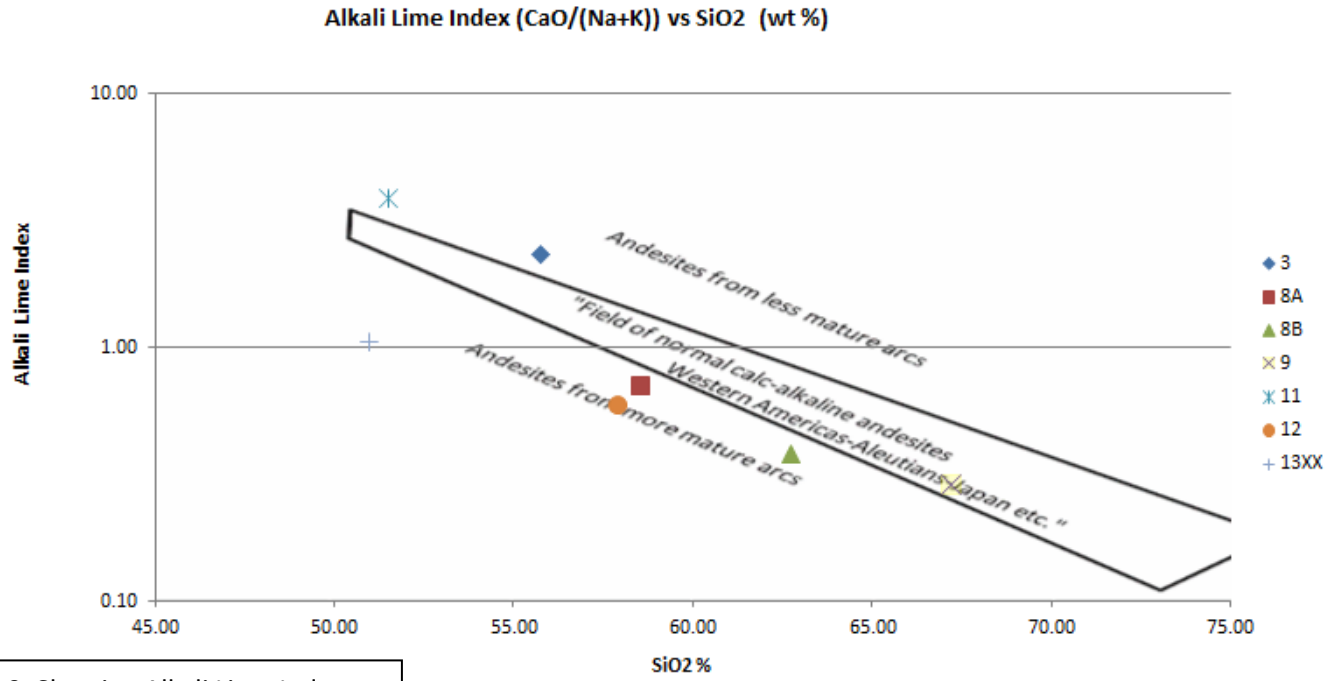

Figure 9. Showing Alkali Lime Index against Silica wt %.

The alkali lime index is designed to define the maturity of the arc from which the samples originated. Again potassium is involved in the creation of this graph so it may be affected in some way by alteration. However we see a repeat of the two separate series also seen in figure 7, with samples 3 and 11 originating from a mature arc complex and 4 samples originating from an immature arc complex. Sample 9 is towards the immature end of a normal island arc signature, so it could possibly be included with the 4 immature arc samples.

AFM Diagram

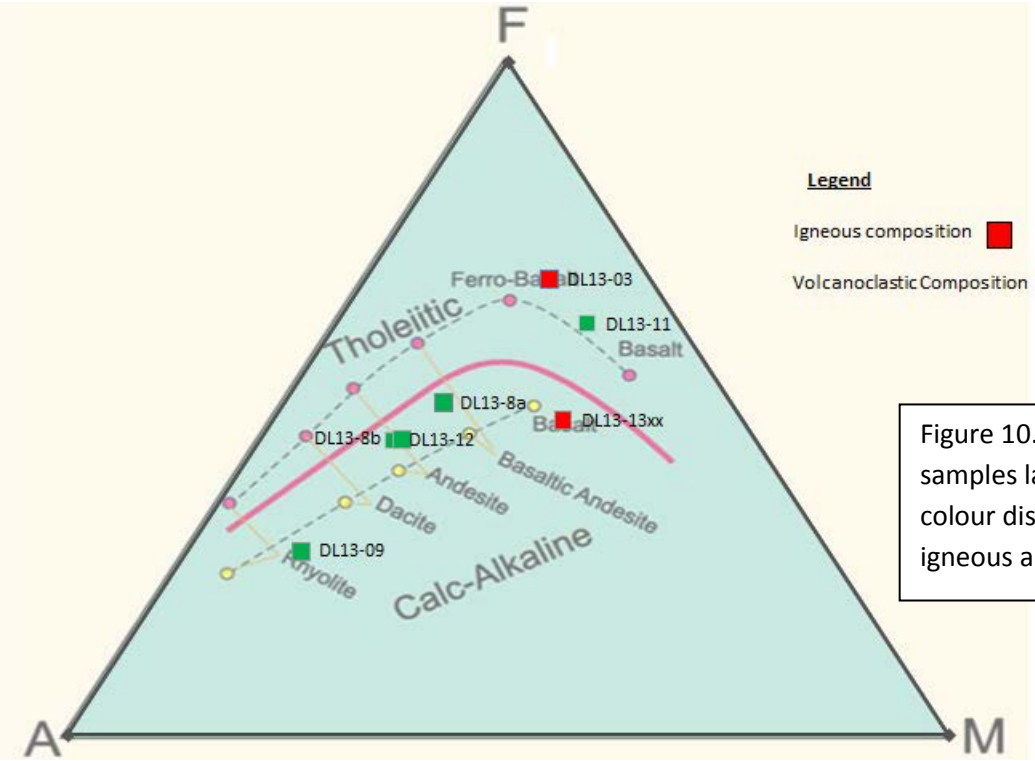

Figure 10. AFM plot with the samples labelled by number and colour distinguishing between igneous and volcanoclastic rocks.

Samples 3 and 11 plot high up along the tholeiitic trend showing a high iron content and are quite separate from the other five samples in the data set. When sample 13XX is disregarded the remaining 4 samples plot in a relatively clear trend close to what is considered the calc-alkaline trend. However if 13XX is included the samples form the distinctive curved trend of the tholeiitic series, but plots between the 'true' calc alkaline and tholeiitic trends. There is no distinction to be made from the igneous and volcanoclastic samples in this graph.

Fe/MgO against SiO_2 (wt %)

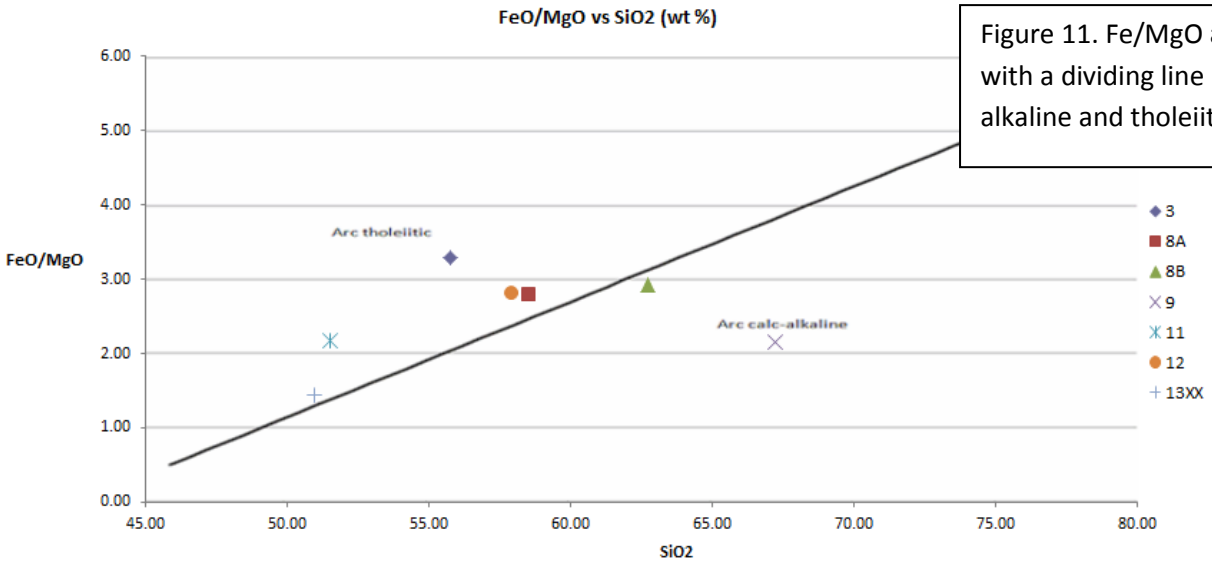

Figure 11. Fe/MgO against SiO_2 (wt %) with a dividing line between calc-alkaline and tholeiitic arc signatures.

This plot confirms many of the observations seen in figure 10, however in this plot instead of samples 3 and 11 being separate to the other five it is samples 13XX and 11 that plot away from the trend of the remaining five. The remaining samples are plotting in a relatively clear trend progressing from arc tholeiite to arc calc-alkaline with increasing silica content. This can be seen in figure 10 as well, even though sample 3 is separated by its low alkali content from the rest of the samples that form a trend, it does conform.

Th/Ta against Ta/Yb- Tectonic Setting DiscriminationPlot

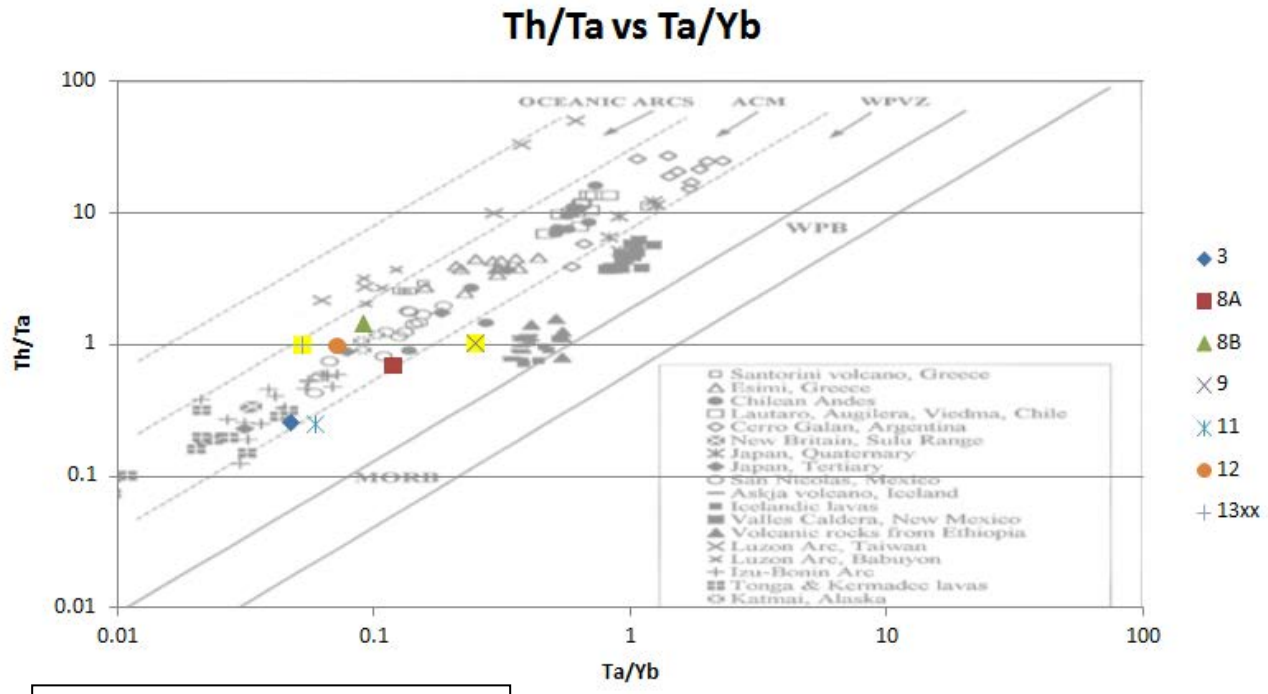

Figure 12. Tectonic discrimination plot. ACM- Active Continental Margin. WPVZ-Within Plate Volcanic Zones. WPB-Within Plate Basalts.

This plot is unexpected in terms of the tectonic setting it places the samples. With the majority of samples plotting in the active continental margin not the oceanic arc field this goes against what was claimed by (KOS'KO M. , 2009) which would have seen the samples plotting in the ocean arc field. However the same occurrence has been recorded with the samples of the Izu Bonin Arc, another oceanic arc, where the samples collected plot in the adjacent field. This is due to the initial ratios of the elements plotted being modified by a number of processes such as a the addition of a depleted mantle component, the influence of volcanogenic sediments or subducted fluids (GORTON & SCHANDL, 2000). It is likely that the samples from the De Longs were also affected by one of these processes.

REE Plots

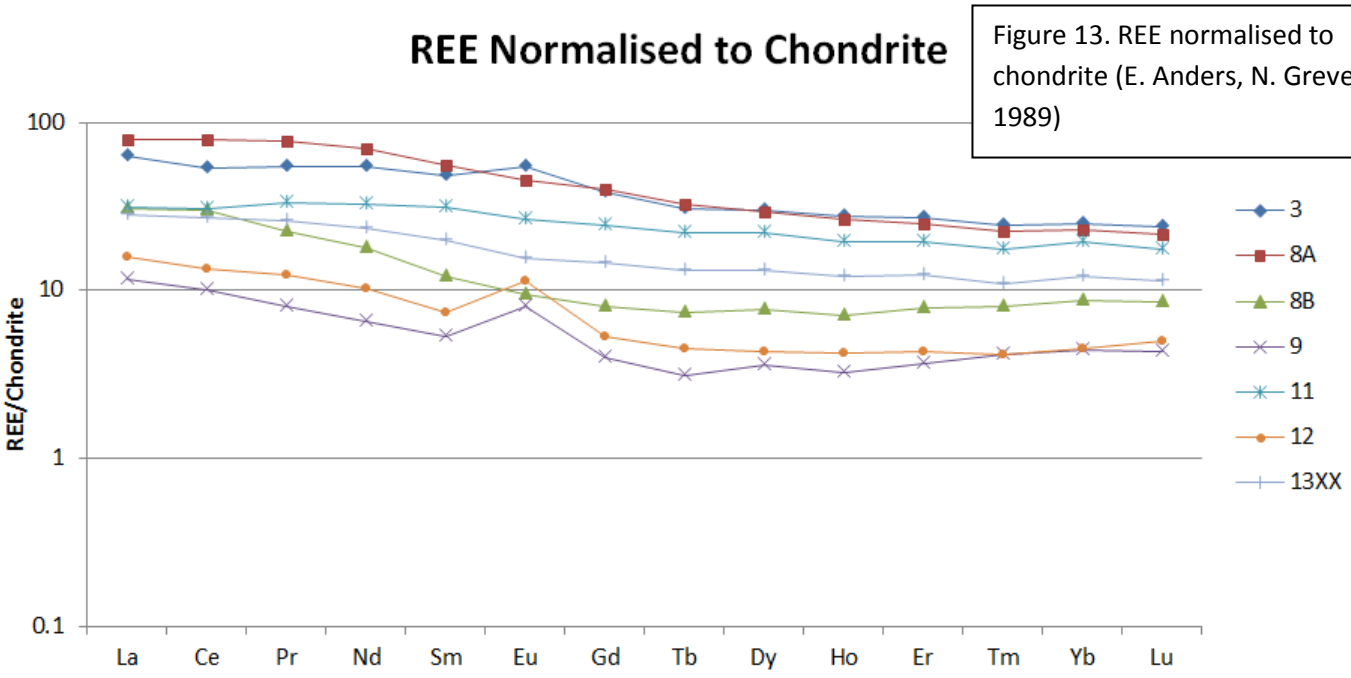

Figure 13. REE normalised to chondrite (E. Anders, N. Grevesse, 1989)

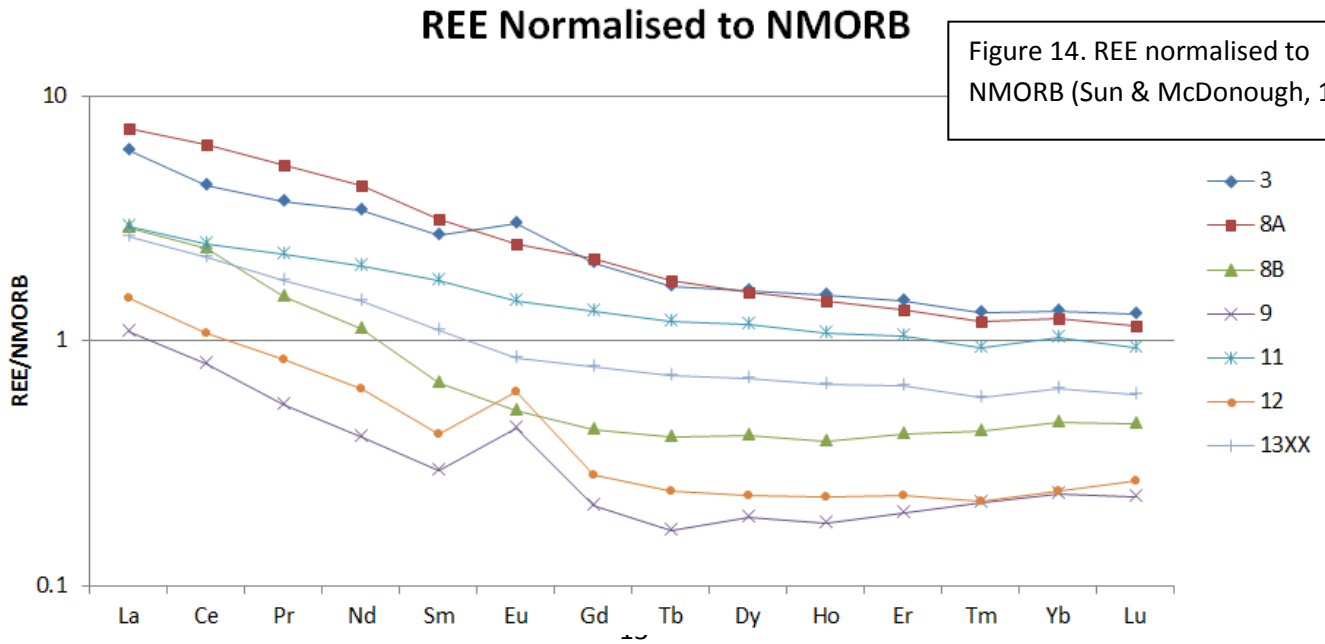

Figure 14. REE normalised to NMORB (Sun & McDonough, 1989)

In the REE plots the trends seen in previous diagrams are not as visible; samples 13XX and 11, identified as a separate series from the other samples in figure 11, have very similar results to each other when normalised to both chondrite and NMORB. All the samples follow a very similar trend of a gentle negative slope which is indicative of fractionation. The HREE elements are all flat showing a lack of fractionation. Most samples are depleted in HREE when compared to MORB however samples 8B, 9 and 12 are more depleted than NMORB in most REE's. Silica content does not seem to have any bearing on whether the sample will be depleted when compared to NMORB. In 3 samples, 12, 9 and 3 there is a positive Eu anomaly indicating higher amounts of plagioclase in these samples.

Multi-Element Plot

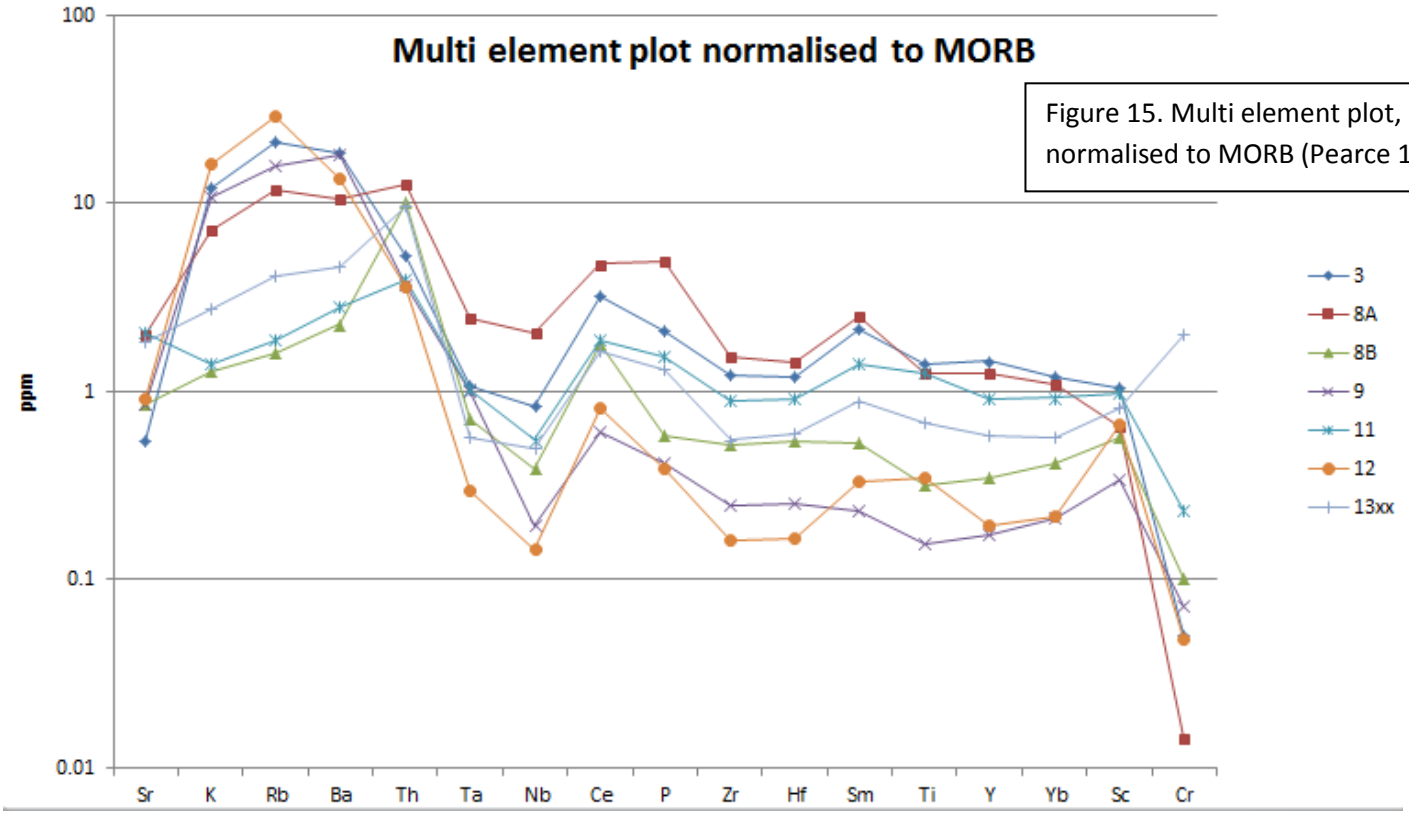

Figure 15. Multi element plot, normalised to MORB (Pearce 1983)

Elemental abundances of the HREE and HFSE elements are generally depleted in comparison to MORB in most of the samples. The incompatible LIL's show strong enrichment compared to MORB in this plot. There is also a decoupling between the HFSE and LIL's in this plot. This combined with a great disparity between fluid mobile elements and fluid immobile elements is a typical signature of arc rocks. The large negative anomaly of Nb and Ta is very characteristic of arc rocks. There is a small positive Sm anomaly in a number of the samples.

Discussion

The first thing to note about these samples is the sample size is very small so coming to conclusions with any great deal of confidence is very difficult. However the rocks that were analysed do seem to offer some insight into the geological history of Henrietta Island with very convincing results.

A number of the rock type discrimination plots were difficult to interpret due to the anomalous nature of the K values due to secondary alteration. Evidence for alteration was very obvious when studying thin sections of the samples, with large amounts of greenschist facies metamorphism. However it is important to note there is a large variation in the composition of the rocks, reflected in figure 7, from mafic to relatively felsic which would indicate a more mature arc as the more felsic rocks are not common in immature arcs (Green, 1980) .

An indication of the source area for these rocks is given in the lack of fractionation in the HREE. The flat signatures of the HREE in all samples indicate there was no garnet at the depth these rocks were sourced from (Verma & Hasenaka, 2004). This would indicate the source to be in the spinel lherzolite zone in the mantle wedge above or relatively close to the subducting oceanic crust. Further evidence for a shallow mantle source is evident in the multi element plot; due the similarities between the NMORB and samples in terms of HREE elements it indicates the source was depleted NMORB type and shallow (Menzies & Chazot, 1995). Evidence for a depleted mantle source is further strengthened due to the plotting outside of the oceanic arc zone in figure twelve. An explanation for this is the influence of a depleted MORB type melt which modifies the trace element ratios (GORTON & SCHANDL, 2000).

A shallow source would indicate a relatively close proximity to the subduction zone, as there would be an abundance of fluids and the seismic zone depth increases further away from the subduction zone. Evidence for fluid interaction is shown in the typical arc signature of the decoupling between the HFSE and LILE elements in the multi element plot, combined with the very large negative Ta, Nb anomaly. Ta and Nb are highly depleted in arc rocks due to their fluid immobility. Therefore as the slab subducts the fluid mobile LILE's are removed during the dewatering of the slab and are available to contribute to melt the overlying mantle and are then registered in the erupted oceanic arc rocks. Whereas Nb and Ta are immobile in fluid and stay constrained within the slab, and are therefore depleted in arc rocks (Pearce & Peate, 1995).

The AFM plot (figure 10) shows the majority of the samples plot between calc-alkaline and tholeiitic trends, which indicates one of two things; either the samples originate from relatively close to the subduction zone in a mature arc or are in fact from different distances from the subduction zone. This is because there is both a temporal and spatial association with the progression from arc tholeiites to calc-alkaline magmas (Green, 1980). A maturing arc complex can explain the close proximity of the samples as opposed to the samples being produced at greater distances from the subduction zone. This theory is compounded by figure 9 which gives both evidence of a mature and immature arc from within our small set of samples.

Conclusion

Henrietta Island is the location of ocean arc derived igneous rocks as samples display typical arc signatures in multi element plots. The samples collected show evidence of being derived from a depleted mantle source as confirmed by trace element analysis and multi element plots. The samples were formed in relatively close proximity to the subduction zone of this island arc, these samples were produced over a time span during which the arc continued to mature. Fluids derived from the subducting oceanic crust were also instrumental in the formation of these rocks.

Further Research

It would be interesting to date these rocks and the surrounding rocks associated with this volcanic arc and link it to the geochemistry. Age data when combined with the geochemistry would be able to provide a definitive answer to whether the samples were produced by a maturing arc in one spot or by the samples being produced at varying distances from the subduction zone.

Bibliography

Dovzhikova, E., Pease, V., & Remizov, D. (2004). Neoproterozoic island arc magmatism beneath the Pechora Basin, NW Russia. *GFF*, 353-362.

GORTON, M. P., & SCHANDL, E. S. (2000). FROM CONTINENTS TO ISLAND ARCS: A GEOCHEMICAL INDEX OF TECTONIC SETTING FOR ARC-RELATED AND WITHIN-PLATE FELSIC TO INTERMEDIATE VOLCANIC ROCKS. *The Canadian Mineralogist*, 1065-1073.

Green, T. (1980). Island arc and continent-building magmatism — A review of petrogenic models based on experimental petrology and geochemistry. *Tectonophysics*, 367-385.

Harris, J. R., Wilkinsona, L., & Grunsky, E. C. (2000). Effective use and interpretation of lithogeochemical data in regional mineral exploration programs: application of Geographic Information Systems GIS technology. *Ore Geology Reviews*, 107–143.

Jenner, G. A., Longerich, H. P., Jackson, S. E., & Fryer, B. J. (1990). ICP-MS — A powerful tool for high-precision trace-element analysis in Earth sciences: Evidence from analysis of selected U.S.G.S. reference samples. *Microanalytical Methods in Mineralogy and Geochemistry*, 133–148.

KOS'KO, M. (2009). *Review of the geology of the New Siberian Islands between the Laptev and the East Siberian Seas, North East Russia.*

KOS'KO, M., LOPATIN, B., & GANELIN, V. (1990). Major Geological Features of the Islands of the East Siberian and Chukchi Seas and the Northern Coast of Chukotka . *Marine Geology*, 349-367.

KUZMICHEV, A., & PEASE, V. (2007). Siberian trap magmatism on the New Siberian Islands: constraints for Arctic Mesozoic plate tectonic reconstructions. *Journal of the Geological Society* , 959-968.

Menzies, M., & Chazot, G. (1995). Fluid processes in diamond to spinel facies shallow mantle. *Journal of Geodynamics*, 387-415.

Pearce, J. A., & Peate, D. W. (1995). Tectonic Implications of the Composition of Volcanic Arc Magmas. *Annual Review Of Earth And Planetary Sciences,* , 251-286.

Verma, S., & Hasenaka, T. (2004). Sr, Nd, and Pb isotopic and trace element geochemical constraints for a veined-mantle source of magmas in the Michoacán-Guanajuato Volcanic Field, west-central Mexican Volcanic Belt. *Geochemical Journal*, 43-65.

Wang, X., Yin, X., Zeng, Z., Yang, B., & Chen, S. (2014). High efficiency determination of trace elements in the geological samples. *Journal of Chinese Mass Spectrometry Society*, 24-31.

Appendix

Table 1. Geochemical data. (Note Fe total is included)

Sample	3	8A	8B	9	11	12	13XX
%							
SiO2	55.76	58.53	62.73	67.19	51.53	57.91	50.97
Al2O3	14.34	16.46	16.02	17.69	14.18	19.63	14.63
CaO	5.66	4.18	2.76	2.16	9.16	4.15	5.81
MgO	4.44	3.24	2.68	1.60	6.46	2.77	8.90
MnO	0.46	0.20	0.14	0.11	0.25	0.22	0.23
P2O5	0.25	0.59	0.07	0.05	0.19	0.05	0.16
Fe tot	14.56	9.03	7.82	3.46	13.99	7.77	12.76
FeO	13.11	8.12	7.04	3.11	12.59	6.99	11.48
Fe2O3	1.46	0.90	0.78	0.35	1.40	0.78	1.28
Na2O	0.67	4.84	7.11	5.88	2.17	4.56	5.12
K2O	1.79	1.08	0.19	1.63	0.21	2.43	0.41
TiO2	2.08	1.86	0.47	0.23	1.86	0.52	1.03
ppm							
Sc	41.57	26.13	22.63	13.70	38.93	26.50	32.50
V	204.33	92.00	124.33	45.17	254.67	75.63	241.00
Cr	12.63	3.59	25.23	18.13	57.83	11.93	502.33
Ni	14.00	3.12	13.97	7.31	28.93	6.62	81.63
Cu	34.80	7.87	13.93	12.37	25.83	5.44	44.53
Ga	19.07	17.53	13.83	15.20	16.33	20.00	12.60
Rb	41.93	23.73	3.18	31.50	3.76	58.27	8.30
Sr	65.33	238.33	103.00	102.00	247.33	110.33	220.00
Y	43.40	37.23	10.41	5.23	27.40	5.85	17.40
Zr	110.67	138.00	46.40	22.33	80.10	14.50	49.57
Nb	2.94	7.16	1.37	0.67	1.93	0.51	1.76
Cs	1.29	1.40	0.36	1.54	0.31	2.01	1.13
Ba	373.67	209.67	45.30	362.67	56.67	270.33	91.10
La	14.90	18.43	7.19	2.71	7.29	3.72	6.69
Ce	32.17	47.53	17.93	6.05	18.57	8.07	16.47
Pr	4.88	6.88	2.01	0.72	2.98	1.11	2.31
Nd	24.80	31.40	8.15	2.96	14.70	4.67	10.60
Sm	7.13	8.20	1.77	0.77	4.61	1.09	2.91
Eu	3.08	2.55	0.53	0.45	1.48	0.63	0.86
Gd	7.64	7.94	1.59	0.78	4.82	1.04	2.89
Tb	1.12	1.18	0.27	0.11	0.80	0.16	0.48
Dy	7.27	7.16	1.86	0.86	5.33	1.06	3.20
Ho	1.54	1.46	0.39	0.18	1.08	0.23	0.67
Er	4.31	3.98	1.24	0.59	3.09	0.69	1.95
Tm	0.60	0.55	0.19	0.10	0.43	0.10	0.27
Yb	4.04	3.74	1.41	0.72	3.14	0.74	1.95
Lu	0.58	0.52	0.21	0.11	0.43	0.12	0.28
Hf	2.89	3.47	1.30	0.61	2.20	0.40	1.42
Ta	0.19	0.44	0.13	0.18	0.18	0.05	0.10
Pb	11.90	8.03	3.74	2.70	2.76	5.84	1.86
Th	1.04	2.54	2.02	0.74	0.79	0.72	1.92
U	0.57	0.61	0.50	0.33	0.24	0.22	0.48